



Measurement of energetic-particle-driven core magnetic fluctuations and induced fast-ion transport

L. Lin, W. X. Ding, D. L. Brower, J. J. Kollner, S. Eilerman et al.

Citation: [Phys. Plasmas](#) **20**, 030701 (2013); doi: 10.1063/1.4798397

View online: <http://dx.doi.org/10.1063/1.4798397>

View Table of Contents: <http://pop.aip.org/resource/1/PHPAEN/v20/i3>

Published by the [American Institute of Physics](#).

Additional information on Phys. Plasmas

Journal Homepage: <http://pop.aip.org/>

Journal Information: http://pop.aip.org/about/about_the_journal

Top downloads: http://pop.aip.org/features/most_downloaded

Information for Authors: <http://pop.aip.org/authors>

ADVERTISEMENT

The advertisement banner features a background of green and white wavy lines. At the top, the 'AIP Advances' logo is shown with a series of orange dots forming an arc above the word 'Advances'. Below the logo, the text 'Special Topic Section: PHYSICS OF CANCER' is written in white on a dark green background. At the bottom, the text 'Why cancer? Why physics?' is written in yellow, and a blue button with the text 'View Articles Now' is positioned to the right.

AIP Advances

Special Topic Section:
PHYSICS OF CANCER

Why cancer? Why physics? [View Articles Now](#)

Measurement of energetic-particle-driven core magnetic fluctuations and induced fast-ion transport

L. Lin,¹ W. X. Ding,¹ D. L. Brower,¹ J. J. Koliner,² S. Eilerman,² J. A. Reusch,² J. K. Anderson,² M. D. Nornberg,² J. S. Sarff,² J. Waksman,² and D. Liu³

¹Department of Physics and Astronomy, University of California Los Angeles, Los Angeles, California 90095, USA

²Department of Physics, University of Wisconsin–Madison, Madison, Wisconsin 53706, USA

³Department of Physics and Astronomy, University of California Irvine, Irvine, California 92697, USA

(Received 9 February 2013; accepted 6 March 2013; published online 22 March 2013)

Internal fluctuations arising from energetic-particle-driven instabilities, including both density and radial magnetic field, are measured in a reversed-field-pinch plasma. The fluctuations peak near the core where fast ions reside and shift outward along the major radius as the instability transits from the $n=5$ to $n=4$ mode. During this transition, strong nonlinear three-wave interaction among multiple modes accompanied by enhanced fast-ion transport is observed. © 2013 American Institute of Physics. [<http://dx.doi.org/10.1063/1.4798397>]

In toroidal plasma confinement devices, energetic particles are produced by radio-frequency heating, neutral beam injection (NBI), and fusion reactions. Large populations of energetic particles can drive Alfvénic instabilities, which degrade confinement performance and even cause concentrated fast ion losses that damage internal vacuum components.^{1,2} Energetic-particle-driven instabilities have been extensively studied in tokamaks, spherical tokamaks, and stellarators,² but have only recently been observed in a reversed-field pinch (RFP).^{3–5} Unique features of a RFP lead to a considerably different environment for energetic particles with respect to other magnetic configurations. For instance, larger magnetic shear in a RFP tends to stabilize instabilities. However, weaker toroidal magnetic field results in larger β_f (ratio of energetic particle pressure to magnetic pressure), thereby providing increased drive for instability.⁶

Magnetic fluctuations play an important role in the interaction between Alfvénic instabilities and energetic particles as they can lead to convective and diffusive fast-ion losses.^{7,8} Detailed information of their amplitude and structure permits the computation of fast-ion transport. Furthermore, the associated structural dynamics are critical to understanding mode saturation and damping.⁹ However, direct measurement of energetic-particle-driven internal magnetic fluctuations remains elusive due to the difficulty of accessing the high-temperature plasma interior. In addition, these instabilities are typically more spatially localized when compared to ideal kink or resistive tearing modes, thereby challenging diagnostic capabilities.

This letter presents the first direct experimental measurement of internal magnetic fluctuations associated with energetic-particle-driven instabilities in a high-temperature plasma. Internal radial magnetic field fluctuations, with frequency ~ 90 kHz and rms amplitude 2.0 ± 1.7 G, are directly measured by Faraday-effect polarimetry in the Madison Symmetric Torus (MST) RFP.¹⁰ Along with magnetic fluctuations, simultaneously measured density fluctuations exhibit a dynamically evolving and asymmetric spatial structure that peaks near the core where fast ions reside and shifts outward along the major

radius as the instability evolves. Furthermore, measurements reveal strong nonlinear three-wave coupling among multiple modes that correlate with enhanced fast-ion transport.

The experiments are conducted in MST,⁹ a toroidal device with major radius $R_0 = 1.5$ m and minor radius $a = 0.5$ m. All data are collected in standard (multiple helicity) deuterium RFP plasmas with toroidal current 300 kA, line-averaged electron density $0.7 \times 10^{19} \text{ m}^{-3}$, core electron temperature ~ 260 eV, and edge safety factor $q_a = 0$. A 1 MW hydrogen beam at 25 keV is injected tangentially in the direction of the plasma current. TRANSP modeling¹¹ predicts a centrally peaked (within ± 0.1 m of the magnetic axis) fast ion density profile with the core fast-ion $\beta_f \sim 7\%$, exceeding the core thermal plasma $\beta_0 \sim 2\%$.

The primary internal fluctuation diagnostic is an interferometry-polarimetry system, which measures line-integrated density and Faraday effect, including both equilibrium and fluctuating quantities.¹² This laser-based system, at the wavelength $\lambda_0 = 432 \mu\text{m}$, consists of 11 vertically viewing chords (separation ~ 8 cm) covering most of the plasma cross section and located toroidally $\sim 160^\circ$ from the neutral beam injector. The measured Faraday effect (Ψ) is given by $\Psi = c_F \int n_e B_z dz$, where $c_F = 2.62 \times 10^{-13} \lambda_0^2$, n_e is the electron density, B_z is the magnetic field parallel to the beam, and z is the plasma path length along the probe beam, all in MKS units. Along the same chord, interferometry and collective far-forward scattering from electron density fluctuations (\tilde{n}_e) are simultaneously observed. Fluctuation wavenumbers are resolved by using poloidally and toroidally distributed external magnetic (Mirnov) coils.

Evidence for energetic-particle-driven instabilities is shown in Fig. 1(a), by comparing far-forward scattering measurements for discharges with and without NBI for the chord at $R - R_0 = -0.02$ m. A coherent mode at ~ 90 kHz is only observed in NBI-heated plasmas, indicating a fast-ion driving mechanism. This coherent mode is barely visible on the edge chords ($|R - R_0| \geq 0.28$ m), suggesting a core-localized structure. The lower-frequency (< 30 kHz) fluctuation peak corresponds to a tearing mode whose frequency is

upshifted from 15 kHz to 28 kHz in plasmas with NBI. In addition, broadband fluctuations up to 300 kHz, with frequencies also upshifted during NBI, appear on the scattering signal. The frequency upshift results from the external torque induced by the co-injected NBI acting to increase the core toroidal flow from 28 km/s to 45 km/s, thereby Doppler-shifting the frequency of measured fluctuations.

The NBI-driven mode at ~ 90 kHz is also detected by the external magnetic coils.⁵ The mode is bursty and rotates in the beam injection direction with the toroidal mode number $n = 5$ and the poloidal number $m = 1$. The measured frequency linearly depends on the beam-ion velocity while remaining significantly below the predicted toroidal Alfvén eigenmode (TAE) gap.⁵ These features resemble those of the energetic particle mode (EPM) in tokamaks.¹³ To extract its temporal evolution, a bandpass filter from 60 to 120 kHz is employed. The time trace of an $n = 5$ burst is shown in Fig. 1(b), where $t = 0$ ms corresponds to the peak of the mode. Each $n = 5$ burst has a duration ~ 0.06 ms, corresponding to ~ 160 Alfvén times a/v_A , where v_A is the Alfvén velocity at the plasma core. The peak of the $n = 5$ mode provides a time marker to combine many similar bursts for the purpose of ensemble analysis. Except for Fig. 1(b), all results presented in this letter are obtained after ensembling over 1000 similar bursts. The $n = 5$ density fluctuation is extracted by correlating the interferometry measurement with the spatially Fourier decomposed fluctuations from the magnetic coil array. Figure 1(c) shows the spectrogram of the $n = 5$ line-integrated density fluctuations ($\int \tilde{n}_e dz$) at $R - R_0 = -0.02$ m. A mode at 90 kHz with the duration ~ 0.06 ms is clearly visible, consistent with the far forward scattering and external coil measurements.

Multi-chord interferometry reveals the spatial structure of density fluctuations. As shown in Fig. 2(a), the $n = 5$ density fluctuation, obtained after bandpass filtering and averaging from -0.1 to 0.1 ms, peaks in the plasma core where the fast

ions reside. This structure is very different from that of the global tearing mode which peaks near the plasma edge where the equilibrium density gradient is maximum.¹⁴ From the peak of $\int \tilde{n}_e dz$ at $R - R_0 \sim -0.02$ m, the estimated density fluctuation level ($\int \tilde{n}_e dz / \int n_{e0} dz$ where n_{e0} is the equilibrium electron density) is $\sim 0.4\%$, comparable to tokamak observations.¹⁵ There is also a strong inboard and outboard asymmetry (peaking on the inboard side), resembling that of an antiballooning density fluctuation observed on tokamaks.¹⁶

Internal radial magnetic fluctuations driven by fast ions are also measured for the first time by the Faraday-effect polarimetry technique. Faraday-effect fluctuations ($\tilde{\Psi} = \tilde{\Psi}_{\tilde{n}} + \tilde{\Psi}_{\tilde{b}_z}$) contain contributions from both density fluctuation ($\tilde{\Psi}_{\tilde{n}} = c_F \int \tilde{n}_e B_{z0} dz$) and magnetic fluctuation ($\tilde{\Psi}_{\tilde{b}_z} = c_F \int n_{e0} \tilde{b}_z dz$), where B_{z0} and \tilde{b}_z are the equilibrium and fluctuating magnetic field along the probe beam, respectively. As shown in Fig. 2(c), similar to the interferometry measurements, the profile of Faraday-effect fluctuations also peaks in the plasma interior and is asymmetric across the magnetic axis. A line-averaged magnetic fluctuation amplitude, $\tilde{b}_z = \tilde{\Psi}_{\tilde{b}_z} / (c_F \int n_{e0} dz)$, can be extracted by combining interferometry and polarimetry measurements and properly subtracting $\tilde{\Psi}_{\tilde{n}}$ from $\tilde{\Psi}$. For the central chord, \tilde{b}_z is dominated by radial magnetic fluctuations (\tilde{b}_r) from the plasma core due to both the magnetic geometry and the equilibrium density weighting.¹¹ For the chord at $R - R_0 = 0.06$ m, $\tilde{\Psi} \sim (4 \pm 3) \times 10^{-3}$ deg, much larger than $\tilde{\Psi}_{\tilde{n}} \sim 0.3 \times 10^{-3}$ deg, giving the magnetic fluctuation amplitude $\tilde{b}_r \sim \tilde{b}_z \sim 2.0 \pm 1.7$ G or $\tilde{b}_r/B_0 \sim (7 \pm 5) \times 10^{-4}$ near the plasma center. Similar analysis for the chord at $R - R_0 = -0.02$ m leads to $\tilde{b}_r \sim \tilde{b}_z \sim 2.5 \pm 1.5$ G. For the edge chord at $R - R_0 = -0.32$ m, $\tilde{\Psi} \sim (6 \pm 3) \times 10^{-3}$ deg and $\tilde{\Psi}_{\tilde{n}} < 2.5 \times 10^{-3}$ deg, allowing us to estimate a lower bound of $\tilde{b}_z > 0.6$ G, roughly consistent with $\tilde{b}_\theta \sim 0.6$ G at $r \sim 0.5$ m from the external coils. The edge magnetic fluctuation is approximately four times less than the core radial magnetic fluctuation as expected for the core-localized fast-ion drive. Radial magnetic fluctuations also exhibit some asymmetry across the magnetic axis, consistent with the asymmetric density fluctuations, implying a correlation between them. One possible explanation for an asymmetric

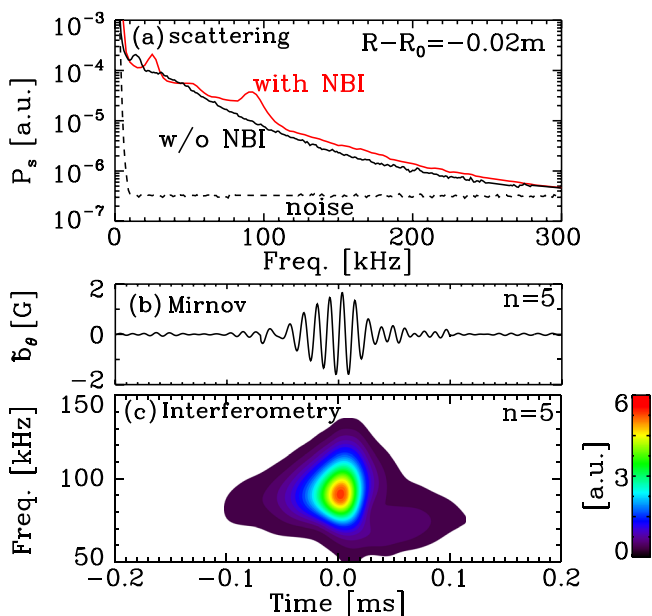


FIG. 1. (a) Frequency spectra of far-forward scattering at $R - R_0 = -0.02$ m; (b) a single $n = 5$ burst from the Mirnov coils; (c) spectrogram of $n = 5$ interferometry measurements at $R - R_0 = -0.02$ m.

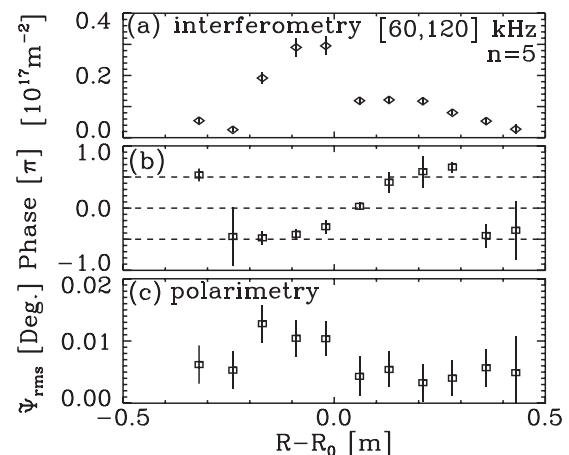


FIG. 2. Profile of (a) rms amplitude and (b) phase of line-integrated density fluctuations, and (c) rms amplitude of Faraday-effect fluctuations for the $n = 5$ mode.

fluctuation profile is an asymmetric fast-ion density distribution leading to an asymmetric drive.

Further quantitative analysis indicates that the observed density fluctuations can arise from magnetic fluctuations. Measurements also suggest that \tilde{n}_e is dominated by compression in the core while significant \tilde{n}_e results from advection toward the edge. This can be established using the electron continuity equation, where \tilde{n}_e arising from the magnetic field line displacement (ξ) is written as $\tilde{n}_e = -n_{e0} \nabla \cdot \xi - \xi \cdot \nabla n_{e0}$. The first term is related to compression and the second to advection.¹⁴ The measured $\int \tilde{n}_e dz$ peaks at $R - R_0 = -0.02$ m, where n_{e0} is rather flat and its gradient is small, $\partial n_{e0} / \partial r \leq 2 \times 10^{19} \text{ m}^{-4}$. In order to balance the observed density fluctuation level $\sim 0.4\%$ at $r \sim 0.07$ m with radial compression ($-n_{e0} \nabla \cdot \xi \sim -2n_{e0} \xi_r / r$, where $\partial \xi_r / \partial r \sim \xi_r / r$ is assumed), a radial displacement $\xi_r \sim 1.5 \times 10^{-4}$ m is required. Under the ideal MHD assumption, this yields $\tilde{b}_r \sim (\vec{B} \cdot \nabla) \xi_r \sim 1.6$ G, a value that is roughly consistent with $\tilde{b}_r \sim 2.5 \pm 1.5$ G from Faraday-effect measurements. However, in order to account for \tilde{n}_e solely by advection ($-\xi_r \partial n_{e0} / \partial r$), $\xi_r > 1.4 \times 10^{-3}$ m is necessary, requiring $\tilde{b}_r > 14$ G. This is well above the direct Faraday-effect measurements. Toward the plasma edge, the contribution from advection is expected to increase due to the increasing $\partial n_{e0} / \partial r$. The estimated density fluctuation level at $r \sim 0.38$ m is $\sim 0.2\%$ from Fig. 2(a). Balancing \tilde{n}_e with $-\xi_r \partial n_{e0} / \partial r$ leads to $\xi_r \sim 1.0 \times 10^{-4}$ m and subsequently $\tilde{b}_\theta / B_\theta \sim -\xi_r (\partial B_\theta / \partial r) / B_\theta \sim 2 \times 10^{-4}$ near the edge, where B_θ and \tilde{b}_θ are equilibrium and fluctuating poloidal magnetic field, respectively. This value is comparable to $\tilde{b}_\theta / B_\theta \sim 4 \times 10^{-4}$ at $r \sim 0.5$ m from the external coil measurements, indicating that \tilde{n}_e arises largely from advection near the plasma edge.

The phase profile of density fluctuations also supports that the dominant origin of \tilde{n}_e switches from compression in the core to advection toward the edge. As shown in Fig. 2(b), the phase of $\int \tilde{n}_e dl$ exhibits π shift across the magnetic axis ($R - R_0 \sim 0.05$ m), consistent with the $m = 1$ feature determined from the edge coil measurements. An additional π shift occurs ~ 0.25 m away from the magnetic axis, which can be explained by the increasing contribution from advection ($-\xi_r \partial n_{e0} / \partial r$) towards the edge. Since $\partial n_{e0} / \partial r < 0$, the sign of $-\xi_r \partial n_{e0} / \partial r$ is opposite to $-n_{e0} \nabla \cdot \xi$ under the

assumption that ξ_r retains the same sign across the minor radius.

In addition to the $n = 5$ mode at 90 kHz, two other modes are also observed during NBI: an $n = 4$ mode at 150 kHz and an $n = -1$ mode at 65 kHz. The temporal and spatial evolution of density fluctuations associated with these modes is shown in Fig. 3. The peak of the $n = 4$ density fluctuation [Fig. 3(c)] is $\sim 10\%$ of that of the $n = 5$ density fluctuation and also occurs ~ 0.03 ms later in time. In addition, the structure of the $n = 4$ density fluctuation peaks further outboard than that of the $n = 5$ density fluctuations. Previous work established that the frequency of the $n = 4$ mode exhibits an Alfvénic scaling.⁵ The $n = -1$ density fluctuation [Fig. 3(b)] peaks even further outboard and occurs when both the $n = 4$ and $n = 5$ modes are large.

Both the toroidal mode numbers and frequencies of the $n = 5$, $n = 4$, $n = -1$ modes satisfy the three-wave matching condition: $f_{n=5} = f_{n=4} - f_{n=-1}$. Figure 4(a) shows the temporal evolution of edge poloidal magnetic fluctuations for the three modes, where the $n = 5$ mode not only has a larger amplitude than the $n = 4$ and $n = -1$ modes but also occurs earlier in time, consistent with the core density fluctuation measurements. Significant bicoherence is measured near the peak of the $n = 5$ mode, as shown in Fig. 4(b), indicating strong nonlinear three-wave coupling.¹⁷ One possible explanation is that the $n = 5$ mode causes fast-ion transport as it grows, which leads to saturation and depletion of the $n = 5$ mode as exhibited by its bursty nature [Fig. 1(c)]. In this process, the fast ions are scattered out of resonance and displaced outward, triggering the $n = 4$ mode, while the $n = -1$ mode may be nonlinearly energized through the interaction between the $n = 5$ and $n = 4$ modes. The associated energy redistribution among multiple modes may play an important role in the mode saturation. Similar processes have been demonstrated in the numerical simulation of bursting Alfvén instabilities in tokamaks.¹⁸

Significant fast-ion transport during the NBI-driven modes is revealed through two methods. The first monitors the fast-ion distribution function using a high-energy (up to 45 keV) neutral particle analyzer (NPA),¹⁹ which measures the product of fast ions exchanging charge with background neutrals. In this experiment, the NPA view is tangential and

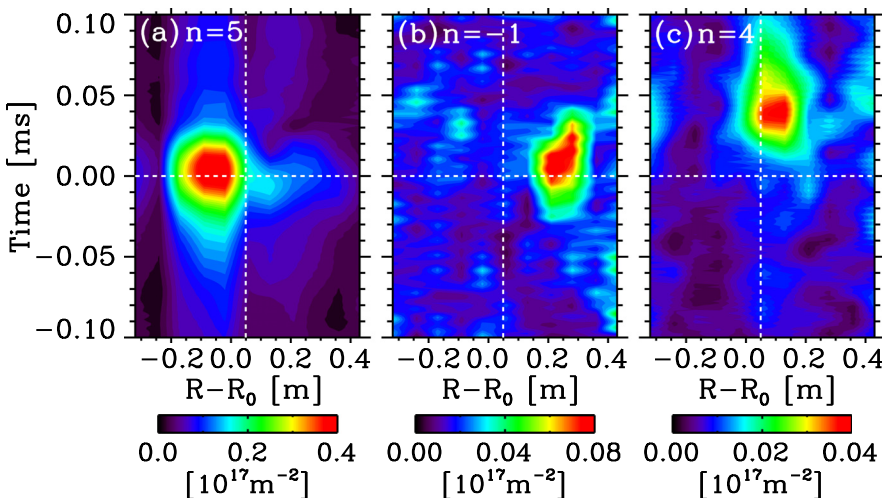


FIG. 3. Temporal evolution of line-integrated density fluctuation profiles associated with the (a) $n = 5$, (b) $n = 4$, and (c) $n = -1$ modes.

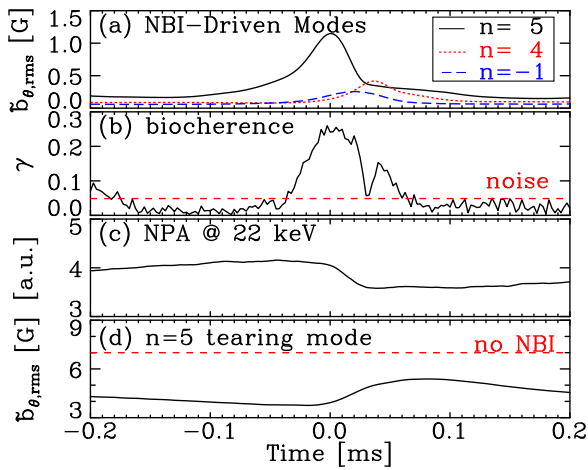


FIG. 4. Temporal evolution of (a) rms amplitudes of edge magnetic fluctuations for the $n=5$, $n=4$, and $n=-1$ modes; (b) their bicoherence; (c) neutral particle analyzer (NPA) signal; and (d) rms amplitude of the $n=5$ tearing mode, where the horizontal dashed line denotes its rms amplitude in non-NBI plasmas.

sensitive to circulating ions. As shown in Fig. 4(c), the NPA signal at 22 keV (near the beam energy at 25 keV) decreases by $\sim 14\%$ following the NBI-driven bursts, while no significant change of background neutrals is detected, indicating beam-ion loss or redistribution. The second method is less direct and involves the temporal dynamics of the global tearing mode. NBI has been observed to reduce the amplitude of the innermost-resonant tearing mode by up to 50%, as shown in Fig. 4(d) for the $n=5$ tearing mode. However, the tearing mode amplitude increases when the NBI-driven mode peaks; hence, the suppression from NBI decreases, consistent with fast ion loss/redistribution. Interestingly, fast-ion transport occurs when the nonlinear coupling among multiple NBI-driven modes reaches maximum, indicating a correlation between fast-ion redistribution and nonlinear three-wave interactions.

In summary, core magnetic fluctuations of energetic-particle-driven instabilities are directly measured in a RFP plasma with relative fluctuation level $\bar{b}_r/B_0 \sim (7 \pm 5) \times 10^{-4}$. The structure of associated density fluctuations dynamically evolves and shifts outward along the major radius as the dominant mode transits from the stronger $n=5$ to the weaker $n=4$ mode. During this process, nonlinear three-wave

interactions occur along with enhanced fast-ion transport, suggesting their important role in the mode transition and saturation.

The authors wish to thank the MST group for their support and contributions to this research. This work is supported by U.S. Department of Energy.

- ¹A. Fasoli, C. Gormenzano, H. L. Berk, B. Breizman, S. Briguglio, D. S. Darrow, N. Gorelenkov, W. W. Heidbrink, A. Jaun, S. V. Kononov, R. Nazikian, J.-M. Noterdaeme, S. Sharapov, K. Shinohara, D. Testa, K. Tobita, Y. Todo, G. Vlad, and F. Zonca, *Nucl. Fusion* **47**, S264 (2007).
- ²W. W. Heidbrink, *Phys. Plasmas* **15**, 055501 (2008).
- ³G. Regnoli, H. Bergsaker, E. Tennfors, F. Zonca, E. Martines, G. Serianni, M. Spolaore, N. Vianello, M. Cecconello, V. Antoni, R. Cavazzana, and J.-A. Malmberg, *Phys. Plasmas* **12**, 042502 (2005).
- ⁴S. Spagnolo, M. Zuin, F. Auremma, R. Cavazzana, E. Martines, M. Spolaore, and N. Vianello, *Nucl. Fusion* **51**, 083038 (2011).
- ⁵J. J. Koliner, C. B. Forest, J. S. Sarff, J. K. Anderson, D. Liu, M. D. Nornberg, J. Waksman, L. Lin, D. L. Brower, W. X. Ding, and D. A. Spong, *Phys. Rev. Lett.* **109**, 115003 (2012).
- ⁶G. Y. Fu and J. W. Van Dam, *Phys. Fluids B* **1**, 1949 (1989).
- ⁷K. Nagaoka, M. Isobe, K. Toi, A. Shimizu, A. Fujisawa, S. Ohshima, H. Nakano, M. Osakabe, Y. Todo, T. Akiyama, Y. Nagashima, C. Suzuki, S. Nishimura, Y. Yoshimura, K. Matsuoka, and S. Okamura, *Phys. Rev. Lett.* **100**, 065005 (2008).
- ⁸M. García-Muñoz, N. Hicks, R. van Voornveld, I. G. J. Classen, R. Bilato, V. Bobkov, M. Bruedgam, H.-U. Fahrbach, V. Igochine, S. Jaemsa, M. Maraschek, and K. Sassenberg, *Phys. Rev. Lett.* **104**, 185002 (2010).
- ⁹B. N. Breizman and S. E. Sharapov, *Plasma Phys. Controlled Fusion* **53**, 054001 (2011).
- ¹⁰R. N. Dexter, D. W. Kerst, T. W. Lovell, S. C. Prager, and J. C. Sprott, *Fusion Technol.* **19**, 131 (1991).
- ¹¹R. Goldston, D. McCune, H. Towner, S. Davis, R. Hawryluk, and G. Schmidt, *J. Comput. Phys.* **43**, 61 (1981).
- ¹²W. X. Ding, D. L. Brower, S. D. Terry, D. Craig, S. C. Prager, J. S. Sarff, and J. C. Wright, *Phys. Rev. Lett.* **90**, 035002 (2003).
- ¹³Y. Todo, *Phys. Plasmas* **13**, 082503 (2006).
- ¹⁴N. E. Lanier, D. Craig, J. K. Anderson, T. M. Biewer, B. E. Chapman, D. J. Den Hartog, C. B. Forest, S. C. Prager, D. L. Brower, and Y. Jiang, *Phys. Plasmas* **8**, 3402 (2001).
- ¹⁵M. A. Van Zeeland, G. J. Kramer, M. E. Austin, R. L. Boivin, W. W. Heidbrink, M. A. Makowski, G. R. McKee, R. Nazikian, W. M. Solomon, and G. Wang, *Phys. Rev. Lett.* **97**, 135001 (2006).
- ¹⁶R. Nazikian, G. J. Kramer, C. Z. Cheng, N. N. Gorelenkov, H. L. Berk, and S. E. Sharapov, *Phys. Rev. Lett.* **91**, 125003 (2003).
- ¹⁷N. A. Crocker, W. A. Peebles, S. Kubota, E. D. Fredrickson, S. M. Kaye, B. P. LeBlanc, and J. E. Menard, *Phys. Rev. Lett.* **97**, 045002 (2006).
- ¹⁸S. Briguglio, G. Fogaccia, G. Vlad, F. Zonca, K. Shinohara, M. Ishikawa, and M. Takechi, *Phys. Plasmas* **14**, 055904 (2007).
- ¹⁹S. Eilerman, J. K. Anderson, J. A. Reusch, D. Liu, G. Fiksel, S. Polosatkin, and V. Belykh, *Rev. Sci. Instrum.* **83**, 10D302 (2012).